2009-0947

47th AIAA Aerospace Sciences Meeting, 5–8 January 2009, Orlando, FL

Assessment of Subgrid-Scale Models and Shock-Confining Filters in Large-Eddy Simulation of Highly Compressible Isotropic Turbulence

Nathan E. Grube* and M. Pino Martín†

Princeton University, Princeton, NJ 08544 USA

Velocity fluctuations in highly compressible turbulent flows can lead to the formation of transient shocklets, while boundary conditions and flow geometries can result in stronger, more permanent shocks, as in shock-wave/turbulent boundary layer interactions. Thus, large-eddy simulation (LES) of these flows requires shock-capturing. Standard linear filters that are used in LES cause undesirable behavior such as smearing or Gibbs oscillations near shocks and other discontinuities. We assess a shock-confining filter (SCF) that behaves like a linear filter in smooth turbulent regions and adapts near discontinuities to avoid oscillations and lessen numerical smearing. Simulations of a shocktube problem and forced isotropic turbulence show the necessity of SCF. Compressible LES also requires the closure of more terms than incompressible LES, and models for compressible LES are less well-developed than their incompressible counterparts. We compare several closure models in highly compressible turbulence as a first step toward selecting a model for LES of interaction problems. Simulations of decaying isotropic turbulence show that certain models can be accurate while giving computational cost roughly 2.4 times that of DNS on the same coarse grid.

I. Introduction

Most turbulent flows contain such a large range of length and time scales that direct numerical simulation (DNS) of the governing equations is prohibitively expensive. One alternative is large-eddy simulation (LES), in which a spatial filter separates the flow scales into large, resolved scales that are computed directly, and smaller, unresolved scales, the effects of which must be modeled. The filtering into resolved and unresolved scales may be accomplished either by explicitly applying a known filter or by allowing the truncation effects of the grid and finite difference scheme to filter the flow implicitly.[a] In both implicitly and explicitly filtered LES, most popular models for the unclosed terms involve numerically explicit filtering operations. For example, the dynamic model of Germano et al.[1,2] and the the scale-similarity model (SSM) of Bardina et al.,[3] as well as the dynamic mixed model (DMM) formed by combining them,[4] use explicit filtering to isolate the smallest resolved scales of various quantities; and the approximate deconvolution model (ADM) of Stolz and Adams[5–7] uses the repeated application of an explicit filter in order to approximate the inverse of the filtering operation.

Because of the large range of length scales, turbulent flows are most efficiently simulated using high-order-accurate numerical schemes that can accurately approximate derivatives of fluctuations over a large range of wavenumbers. However, in compressible flows containing shock waves and other discontinuities, the uniform application of high-order-accurate linear differencing schemes for approximating the spatial derivatives of the convective fluxes leads to the creation of spurious oscillations in regions where the differencing stencil crosses a discontinuity. Over time, these oscillations can grow, corrupting the solution and ultimately causing antiphysical features, such as negative temperatures, which make it impossible to proceed with

*Graduate Student, Mechanical and Aerospace Engineering Department, Princeton University, AIAA Member.

†Assistant Professor, Mechanical and Aerospace Engineering Department, Princeton University, AIAA Senior Member.

[a]We refer here to using truncation effects to filter the flow, not to model the unclosed terms as would be done in a MILES simulation.

the simulation. A variety of shock-capturing methods have been proposed to avoid the creation of these spurious oscillations. Among them are the essentially non-oscillatory (ENO) method[8,9] and the weighted essentially non-oscillatory (WENO) method[10,11] which measure the local smoothness of the flow and then narrow and bias their differencing stencils where needed in order to avoid high-order-accurate interpolation across discontinuities. By adapting the differencing stencil to avoid interpolation across discontinuities, these methods succeed in greatly reducing or eliminating spurious oscillations.

The thickness of a shock is typically orders of magnitude smaller than even the Kolmogorov scale in a turbulent flow, and so, in order to faithfully simulate the physics of an interaction between turbulence and a shock, the shock should remain as thin relative to the turbulence as possible. Most shock-capturing schemes require about four grid points to resolve a shock. Therefore, even without filtering, shocks are numerically smeared in DNS and LES.

Large-eddy simulation of a shock-containing flow presents a dilemma with regard to filtering in space: on the one hand, we want to remove small turbulent scales from the solution in order to model them and thus lower the computational cost; on the other hand, filtering worsens the numerical smearing of shocks. Furthermore, shocks are governed by principles of gasdynamics, and we do not seek to model them with our closure models that are based on the physics of turbulence. If we simply apply a linear filter in a turbulence model, the difference in properties across a shock may be incorrectly interpreted by the turbulence model as a large fluctuation due to turbulence. Based on these conceptual considerations, we desire not to filter shocks.

(W)ENO methods for computing the convective terms devote significant computational effort to measuring the local smoothness of the flow in order to determine how to adapt the difference stencil at each point. We propose an adaptive shock-confining filter (SCF) which seeks to filter turbulent scales in smooth regions according to a known linear filter function, while at the same time affecting discontinuities as little as possible and keeping them confined to as few grid points as is allowed by the underlying shock-capturing scheme. Because the SCF is used in conjunction with a WENO scheme, the smoothness measurement from the convective terms can be reused, and there is little increase in computational cost due to measuring smoothness.

In addition to the issue of filtering in the vicinity of shocks, LES of compressible flows is in general less well-developed than LES of incompressible flows. One purpose of this paper is to assess the suitability of various subgrid-scale models in highly compressible flows. The second purpose is to assess the suitability of shock-confining filtering for LES of shock-containing flows, particularly in the context of ADM simulations, but also in the context of traditional LES. Section II reviews the governing conservation equations as well as the terms to be modeled in both traditional LES, as exemplified by the dynamic Smagorinsky and dynamic mixed models, and mathematical LES, as exemplified by the approximate deconvolution method. Section III discusses filtering for LES, both traditional linear filters and SCF. A method is presented for constructing an SCF from a general linear filter such that the SCF retains the filter properties necessary for a correct solution of gasdynamics problems. Section IV presents numerical simulations that demonstrate the behavior of the SCF in simulations of gasdynamics flows, as exemplified by the shocktube problem, and in turbulent shocklet-containing flows, as exemplified by decaying isotropic turbulence and forced isotropic turbulence. The computational costs of the models are compared in the decaying isotropic turbulence case. Section V presents general conclusions about shock-confining filters and the models under consideration.

II. Compressible Large-eddy Simulations

The temporal evolution of a fluid flow is governed by conservation laws for mass, momentum and energy, which we will collectively refer to as the Navier-Stokes equations. They can be written as:

$$\frac{\partial \rho}{\partial t} + \frac{\partial}{\partial x_j}\left(\rho u_j\right) = 0 \tag{1a}$$

$$\frac{\partial}{\partial t}(\rho u_i) + \frac{\partial}{\partial x_j}(\rho u_i u_j + p\delta_{ij} - \sigma_{ij}) = 0 \tag{1b}$$

$$\frac{\partial}{\partial t}(E) + \frac{\partial}{\partial x_j}\left[(E+p)u_j + q_j - \sigma_{ij}u_i\right] = 0 \tag{1c}$$

where ρ is density, u_j is velocity in the x_j direction, p is pressure, δ_{ij} is the Kronecker delta, $E = \rho c_v T + \frac{1}{2}\rho u_k u_k$ is total energy, T is temperature, $\sigma_{ij} = 2\mu S_{ij}(U) - \frac{2}{3}\mu\delta_{ij}S_{kk}(U)$ is the viscous stress tensor, μ is viscosity, $S_{ij}(U) = \frac{1}{2}\left(\frac{\partial u_j}{\partial x_i} + \frac{\partial u_i}{\partial x_j}\right)$ is the strain rate tensor, $q_j = -k\frac{\partial T}{\partial x_j}$ is the heat flux, and k is thermal conductivity.

To close the system, we use the perfect gas equation of state $p = \rho RT$; a power law for viscosity (in air) $\mu = \mu_{\text{ref}}(T/T_{\text{ref}})^n$, where $\mu_{\text{ref}} = 1.789 \times 10^{-5} kg/m \cdot s$, $T_{\text{ref}} = 288.2K$, and $n = 0.76$; and an assumption of proportionality between thermal conductivity and viscosity $k = (19/4)R\mu$ (for a diatomic gas).

Most turbulent flows contain such a large range of length and time scales that direct numerical simulation (DNS) of the governing equations is prohibitively expensive. Instead, a spatial filtering operation is employed to separate the flow scales into large, resolved scales that can be computed directly, and smaller, unresolved scales, the effects of which must be modeled. Let us define a low-pass filter in terms of a convolution: $\bar{u} = \int G(\vec{x},\vec{y})u(\vec{y})d\vec{y} \equiv G * u$. In order to simplify the analysis of compressible flows, it is also useful to define a Favre (density weighted) filter as $\tilde{f} = \overline{\rho f}/\overline{\rho}$.

Large-eddy simulations can be categorized as either implicitly filtered or explicitly filtered. Implicitly filtered LES relies on the grid truncation and differencing errors to effectively provide a low-pass filter of unknown shape. Explicitly filtered LES uses a known low-pass filter with a cutoff at lower wavenumbers than the grid Nyquist limit. Thus, in implicit LES, the terms subgrid- and subfilter-scale (SGS and SFS) are interchangeable. In explicit LES, we use "SGS" to refer to scales too small to be represented on the grid, and "SFS" to refer to scales which are representable on the grid but which are not resolved by the filter. The full unclosed or unresolved terms are the sum of the SFS and SGS parts. In analytical discussions where grid truncation and differencing have not been considered, there is no grid filter, and hence for convenience we sometimes call analytical unclosed terms SFS.

The only variables that are available in LES are the filtered conserved variables, $\overline{U}$ or ($\overline{\rho}$, $\overline{\rho u}$, $\overline{\rho v}$, $\overline{\rho w}$, $\overline{E}$), which evolve according to the filtered Navier-Stokes equations. All other quantities associated with the filtered solution (e.g., primitive variables and transport coefficients) can only be approximated as functions of known filtered quantities. This can be accomplished by writing an expression for the desired quantity in terms of exact conserved variables and then substituting filtered conserved variables into this definition. We denote a quantity computed in this way by a check: $f = f(U) \Rightarrow \check{f} = f(\overline{U}) \neq \overline{f}$.

We construct governing equations for LES by applying the filter to the Navier-Stokes equation and then rearranging terms so that the left-hand side has the same operational form as the original Navier-Stokes equations but with resolved variables replacing the full variables:

$$\frac{\partial \bar{\rho}}{\partial t} + \frac{\partial}{\partial x_j}(\bar{\rho}\tilde{u}_j) = 0, \tag{2a}$$

$$\frac{\partial}{\partial t}(\bar{\rho}\tilde{u}_i) + \frac{\partial}{\partial x_j}(\bar{\rho}\tilde{u}_i\tilde{u}_j + \bar{p}\delta_{ij} - \check{\sigma}_{ij}) = -\frac{\partial}{\partial x_j}\tau_{ij}, \tag{2b}$$

$$\frac{\partial}{\partial t}(\overline{E}) + \frac{\partial}{\partial x_j}\left[(\overline{E} + \bar{p})\tilde{u}_j + \check{q}_j - \check{\sigma}_{ij}\tilde{u}_i\right] = -\frac{\partial}{\partial x_j}(\gamma c_v Q_j + \frac{1}{2}J_j - D_j), \tag{2c}$$

where $\check{\sigma}_{ij} = 2\mu S_{ij}(\overline{U}) - \frac{2}{3}\mu\delta_{ij}S_{kk}(\overline{U})$ with $S_{ij}(\overline{U}) = \frac{1}{2}\left(\frac{\partial \tilde{u}_j}{\partial x_i} + \frac{\partial \tilde{u}_i}{\partial x_j}\right)$, and $\check{q}_j = -k\frac{\partial \tilde{T}}{\partial x_j}$.

We have neglected unclosed terms arising from variations in viscosity and thermal conductivity. The viscosity μ and thermal conductivity k are computed based on $\check{T} - \tau_{kk}/(2\bar{\rho}c_v)$. The specific heat at constant volume c_v is taken to be constant here.

The terms to be closed are the SFS stresses $\tau_{ij} = \bar{\rho}(\widetilde{u_i u_j} - \tilde{u}_i\tilde{u}_j)$, the SFS heat flux $Q_j = \bar{\rho}(\widetilde{u_j T} - \tilde{u}_j\tilde{T})$, SFS diffusion of turbulent kinetic energy $J_j = \bar{\rho}(\widetilde{u_j u_k u_k} - \tilde{u}_j\widetilde{u_k u_k})$, and the SFS viscous diffusion of energy $D_j = \bar{\rho}(\overline{\sigma_{ij}u_i} - \check{\sigma}_{ij}\tilde{u}_i)$. By definition we have $\bar{E} \equiv \overline{\rho c_v T} + \frac{1}{2}\overline{\rho u_k u_k} \equiv c_v\bar{\rho}\tilde{T} + \frac{1}{2}\bar{\rho}\widetilde{u_k u_k} \equiv c_v\bar{\rho}\check{T} + \frac{1}{2}\bar{\rho}\tilde{u}_k\tilde{u}_k + \frac{1}{2}\tau_{kk}$.

Martín et al.[12] perform an *a priori* analysis of the unclosed terms in the energy budget for decaying isotropic turbulence with $Re_\lambda = \rho_{\text{avg}}u'_{\text{rms}}\lambda/\mu = 50$ and $M_t = q/a_{\text{avg}} = 0.52$ where q is the root-mean-square fluctuating velocity magnitude and a_{avg} is the average speed of sound. They find that the most important SFS term in the energy equation is the heat flux Q_j and that the contribution from the SFS turbulent diffusion J_j is smaller by approximately a factor of two. The contribution from SFS viscous diffusion D_j is approximately an order of magnitude smaller than that from Q_j. We therefore choose to neglect D_j. We also neglect J_j, in part because its effect is smaller than that of Q_j and in part because models for J_j are less well-developed.

Note that the LES governing equations contain $\tilde{T}$ and $\bar{p}$ which cannot be computed exactly but are related to the known quantities $\breve{T}$ and $\breve{p}$ by $\tilde{T} \equiv \breve{T} - \tau_{kk}/(2\bar{\rho}c_v)$ and $\bar{p} \equiv \breve{p} - (\gamma-1)\tau_{kk}/2$. Thus the trace of a model for τ_{ij} provides approximations for $\tilde{T}$ and $\bar{p}$.

II.A. Traditional LES Models

II.A.1. Dynamic Smagorinsky Model

In traditional compressible LES, we must model the retained unclosed terms τ_{ij} and Q_j. The simplest approach is an eddy diffusivity term for transport of momentum and heat, such as the Smagorinsky[13] model along with a turbulent Prandtl number:

$$\tau_{ij} - \frac{\delta_{ij}}{3}\tau_{kk} \approx C\alpha_{ij}, \tag{3}$$

$$Q_j \approx -\frac{C}{Pr_{\text{turb}}}\alpha_j^T, \tag{4}$$

where

$$\alpha_{ij} = -2\overline{\Delta}^{\,2}\overline{\rho}\left|S(\overline{U})\right|\left(S_{ij}(\overline{U}) - \frac{\delta_{ij}}{3}S_{kk}(\overline{U})\right), \tag{5}$$

$$\alpha_j^T = \overline{\Delta}^{\,2}\overline{\rho}\left|S(\overline{U})\right|\left(\frac{\partial\widetilde{T}}{\partial x_j}\right), \tag{6}$$

$|S_{ij}| = \sqrt{2S_{ij}S_{ij}}$, $\overline{\Delta}$ is the cutoff lengthscale of the filter, and C and Pr_{turb} are model parameters.

We can dynamically compute the model parameters[1,2,14] using a self-similarity assumption between the flow filtered at the $\overline{\cdot}$ level and the flow filtered a second time using a test filter $\widehat{\cdot}$ such that the cutoff lengthscale of the composite filter $\widehat{\overline{\cdot}}$ is twice that of the original filter $\overline{\cdot}$ alone. The test filtering introduces new SFS terms at the test filter level:

$$T_{ij} = \widehat{\overline{\rho}}(\widehat{\overline{u_i}\overline{u_j}} - \breve{\overline{u}}_i\breve{\overline{u}}_j), \tag{7}$$

$$\mathbb{Q}_j = \widehat{\overline{\rho}}\left(\widehat{\overline{T}\overline{u_j}} - \breve{\overline{T}}\breve{\overline{u}}_j\right), \tag{8}$$

where $\breve{\overline{f}} \equiv \widehat{\overline{\rho f}}/\widehat{\overline{\rho}}$ is the Favre filter associated with the composite filter $\widehat{\overline{\cdot}}$. The unclosed stresses at the test filtered level can be related to those at the LES filtered level using the Germano identity:

$$\mathcal{L}_{ij} = T_{ij} - \widehat{\tau_{ij}}, \tag{9}$$

where

$$\mathcal{L}_{ij} \equiv \left(\frac{\widehat{\overline{\rho u_i}\,\overline{\rho u_j}}}{\overline{\rho}}\right) - \frac{\widehat{\overline{\rho u_i}}\,\widehat{\overline{\rho u_j}}}{\hat{\overline{\rho}}} \tag{10}$$

is the "resolved" part of the SFS stress at the $\widehat{\overline{(.)}}$ level and can be computed from known quantities. (Note that the test filter acts on the entire first term, not only the numerator.) Applying the Smagorinsky model to the stresses at both filter levels in (9) yields:

$$\mathcal{L}_{ij} = C\beta_{ij} - \widehat{C\alpha_{ij}}, \tag{11}$$

where

$$\beta_{ij} = -2\widehat{\overline{\Delta}}^{\,2}\widehat{\overline{\rho}}\left|S(\widehat{\overline{U}})\right|\left(S_{ij}(\widehat{\overline{U}}) - \frac{\delta_{ij}}{3}S_{kk}(\widehat{\overline{U}})\right), \tag{12}$$

and $S_{ij}(\widehat{\overline{U}}) = \frac{1}{2}\left(\frac{\partial\breve{\overline{u}}_j}{\partial x_i} + \frac{\partial\breve{\overline{u}}_i}{\partial x_j}\right)$. Assuming that the parameter C can be pulled outside of the test filter operation, we can solve for C:

$$C = \frac{\langle\mathcal{L}_{ij}M_{ij}\rangle}{\langle M_{lk}M_{lk}\rangle}, \tag{13}$$

where

$$M_{ij} = \beta_{ij} - \widehat{\alpha_{ij}}. \tag{14}$$

The angle brackets indicate averaging over homogeneous directions, which, it is hoped, mitigates the incorrectness of pulling C out of the test filter operation. After averaging, the numerator is clipped to zero to eliminate any negative values.

A similar procedure yields a dynamic prediction for the turbulent Prandtl number:

$$\frac{Pr_{\text{turb}}}{C} = \frac{\langle M_k^T M_k^T \rangle}{\langle \mathcal{L}_j^T M_j^T \rangle} \tag{15}$$

where

$$\mathcal{L}_j^T = \left(\widehat{\frac{\overline{\rho T}\,\overline{\rho u_j}}{\overline{\rho}}} \right) - \frac{\widehat{\overline{\rho T}}\,\widehat{\overline{\rho u_j}}}{\hat{\overline{\rho}}}, \tag{16}$$

$$M_j^T = \beta_j^T - \widehat{\alpha_j^T}, \tag{17}$$

and

$$\beta_j^T = \widehat{\overline{\Delta}}^{\,2} \hat{\overline{\rho}} \left| S(\widehat{\overline{U}}) \right| \left(\frac{\partial \breve{\breve{T}}}{\partial x_j} \right). \tag{18}$$

The dynamic Smagorinsky model of Moin et al.[14] included an additional dynamic coefficient for modeling the trace of the SGS stress tensor. By omitting this coefficient, we effectively absorb the SGS turbulent kinetic energy into a modified pressure.[15] According to Comte and Lesieur[15] this has little effect as long as M_t is not too large. For the $M_t \approx 1$ forced simulations considered in this paper, this approximation may be questionable.

II.A.2. Dynamic Mixed Model

The dynamic Smagorinsky model adds an appropriate amount of global dissipation to the flow; however, the model predictions correlate poorly in space with the exact SFS terms in *a priori* studies using DNS data. The scale-similarity model (SSM) of Bardina et al.[3] correlates much better. This model is of the form:

$$\tau_{ij} \approx A_{ij} \equiv \overline{\rho} \left(\widetilde{\widetilde{u}_i \widetilde{u}_j} - \tilde{\tilde{u}}_i \tilde{\tilde{u}}_j \right). \tag{19}$$

The SSM accurately represents the spatial structure of the SFS stresses in *a priori* studies, but it is insufficiently dissipative. Speziale et al.[16] proposed a mixed model composed of a linear combination of an eddy diffusivity model and the SSM. A dynamic mixed model (DMM) was proposed by Vreman et al.[4] The DMM combines the improved spatial correlation of the SSM with the proper global dissipation of the dynamic Smagorinsky model.

This study will take the one-coefficient dynamic mixed model as reported in Martín et al.[12] as representative of traditional LES models. This model can be written:

$$\tau_{ij} \approx C\alpha_{ij} + A_{ij} \tag{20}$$

Because the eddy diffusivity term now models only the difference between the unclosed term τ_{ij} and the SSM term A_{ij}, the dynamic coefficient is calculated from

$$C = \frac{\langle \mathcal{L}_{ij} M_{ij} \rangle - \langle N_{ij} M_{ij} \rangle}{\langle M_{lk} M_{lk} \rangle}, \tag{21}$$

where

$$N_{ij} = B_{ij} - \widehat{A_{ij}} \tag{22}$$

and

$$B_{ij} = \hat{\overline{\rho}} \left(\widetilde{\breve{\breve{u}}_i \breve{\breve{u}}_j} - \breve{\breve{\tilde{u}}}_i \breve{\breve{\tilde{u}}}_j \right) \tag{23}$$

is the SSM term associated with the test filter level.

Similarly, the SFS heat flux is modeled as:

$$Q_j \approx -\frac{C}{Pr_{\text{turb}}}\alpha_j^T + A_j^T, \tag{24}$$

where

$$A_j^T = \overline{\rho}\left(\widetilde{\tilde{T}\tilde{u}_j} - \tilde{\tilde{T}}\tilde{\tilde{u}}_j\right), \tag{25}$$

and the turbulent Prandtl number is computed from

$$\frac{Pr_{\text{turb}}}{C} = \frac{\left\langle M_k^T M_k^T \right\rangle}{\left\langle \mathcal{L}_j^T M_j^T \right\rangle - \left\langle N_j^T M_j^T \right\rangle}, \tag{26}$$

where

$$N_j^T = B_j^T - \widehat{A_j^T} \tag{27}$$

and

$$B_j^T = \widehat{\overline{\rho}}\left(\breve{\tilde{\breve{T}}}\breve{\tilde{u}}_j - \breve{\breve{T}}\breve{\breve{u}}_j\right). \tag{28}$$

II.B. Approximate Deconvolution Method

Another LES closure method is the Approximate Deconvolution Method (ADM) of Stolz and Adams.[5] In this method, the spatially filtered flow solution is approximately defiltered using an iterative application of G in an algorithm proposed by van Cittert.[17] As an approximate inverse to a filter G, we define $Q_N = \sum_{i=0}^{N}(I-G)^i \approx G^{-1}$. Figure 1 shows transfer functions for the simple tophat filter (56) and for the composition of the tophat and its approximate inverse as given by five terms in van Cittert's deconvolution method.

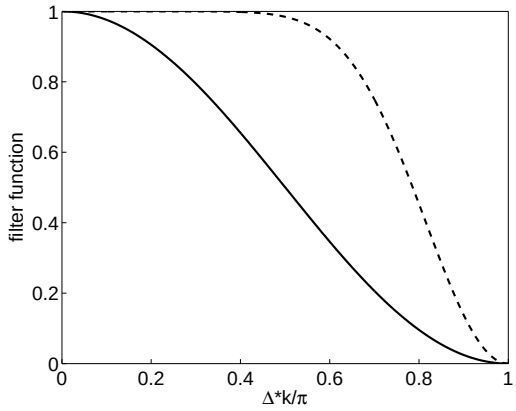

Figure 1. Filter functions for simple tophat filter (———) and composition (– – – –) of simple tophat filter with its approximate inverse as given by five terms in van Cittert's deconvolution method.

The resulting defiltered data $U^\star = Q_N * \overline{U} = Q_N \circ G * U$ are used as an approximation to the exact (unfiltered) flow quantities and are substituted directly into the inviscid flux terms on the left-hand side of the Navier-Stokes equations.

The Navier-Stokes equations can be written in terms of fluxes as:

$$\frac{\partial}{\partial t}\mathbf{U} + \frac{\partial}{\partial x_j}\mathbf{E}_j(\mathbf{U}) + \frac{\partial}{\partial x_j}\mathbf{E}_j^{\text{visc}}(\mathbf{U}) = 0 \tag{29}$$

where

$$\mathbf{U} = \begin{pmatrix} \rho \\ \rho u_1 \\ \rho u_2 \\ \rho u_3 \\ E \end{pmatrix} \equiv \begin{pmatrix} c_1 \\ c_2 \\ c_3 \\ c_4 \\ c_5 \end{pmatrix} \tag{30}$$

is the vector of conserved variables,

$$\mathbf{E}_j(\mathbf{U}) = \begin{pmatrix} \rho u_j \\ \rho u_1 u_j + p\delta_{1j} \\ \rho u_2 u_j + p\delta_{2j} \\ \rho u_3 u_j + p\delta_{3j} \\ (E+p)u_j \end{pmatrix} \tag{31}$$

with $p(\mathbf{U}) = \frac{R}{c_v}\left(c_5 - \frac{1}{2} * \frac{(c_2^2+c_3^2+c_4^2)}{c_1}\right)$ is the vector of inviscid fluxes in the x_j direction, and

$$\mathbf{E}_j^{\text{visc}}(\mathbf{U}) = \begin{pmatrix} 0 \\ -\sigma_{1j} \\ -\sigma_{2j} \\ -\sigma_{3j} \\ q_j - \sigma_{ij}u_i \end{pmatrix} \tag{32}$$

is the vector of viscous fluxes in the x_j direction. We will neglect the unclosed terms arising from the viscous fluxes. Then the LES governing equations can similarly be written

$$\frac{\partial}{\partial t}\overline{\mathbf{U}} + \frac{\partial}{\partial x_j}\mathbf{E}_j(\overline{\mathbf{U}}) + \frac{\partial}{\partial x_j}\mathbf{E}_j^{\text{visc}}(\overline{\mathbf{U}}) = -\frac{\partial}{\partial x_j}\mathbf{T}_j^{\text{full}}, \tag{33}$$

where

$$\mathbf{T}_j^{\text{full}} \equiv \left[\overline{\mathbf{E}_j(\mathbf{U})} - \mathbf{E}_j(\overline{\mathbf{U}})\right]. \tag{34}$$

Traditional SFS models tend to model the full unresolved quantity $\mathbf{T}^{\text{full}}$. In ADM, we compute approximately defiltered variables $\mathbf{U}^\star$, which approximately represent the resolved scales plus the scales that are between the filter cutoff wavenumber and the Nyquist cutoff wavenumber for the grid. In the context of ADM, we call such scales sub-filter scales (SFS) to distinguish them from subgrid scales (SGS) that are smaller than the Nyquist limit for the grid and cannot be represented at all. The full unclosed terms may be decomposed into SFS and SGS parts:

$$\mathbf{T}_j^{\text{full}} = \underbrace{\overline{\mathbf{E}_j(\mathbf{U})} - \overline{\mathbf{E}_j(\mathbf{U}^\star)}}_{\mathbf{T}_j^{SGS}} + \underbrace{\overline{\mathbf{E}_j(\mathbf{U}^\star)} - \mathbf{E}_j(\overline{\mathbf{U}})}_{\mathbf{T}_j^{SFS}}. \tag{35}$$

The second term in $\mathbf{T}^{\text{SFS}}$ is expressed in terms of known, filtered variables. It can be computed exactly. In fact, it cancels with the convective term on the left-hand side. The first term in $\mathbf{T}^{\text{SFS}}$ is also known once $\mathbf{U}^\star$ has been calculated, so it is moved to the left-hand side, leaving only $\mathbf{T}^{\text{SGS}}$ to be modeled:

$$\frac{\partial}{\partial t}\overline{\mathbf{U}} + \frac{\partial}{\partial x_j}\overline{\mathbf{E}_j(\mathbf{U}^\star)} + \frac{\partial}{\partial x_j}\mathbf{E}_j^{\text{visc}}(\overline{\mathbf{U}}) = -\frac{\partial}{\partial x_j}\mathbf{T}_j^{SGS}. \tag{36}$$

II.B.1. Regularization by Relaxation

Stolz et al.[6,7] model the dissipative effect of the SGS terms using relaxation terms with dynamic coefficients to prevent energy from piling up in the subfilter scales. The resulting equations can be written:

$$\frac{\partial}{\partial t}\overline{\mathbf{U}} + \frac{\partial}{\partial x_j}\overline{\mathbf{E}_j(\mathbf{U}^\star)} + \frac{\partial}{\partial x_j}\mathbf{E}_j^{\text{visc}}(\overline{\mathbf{U}}) = -\mathbf{X}, \tag{37}$$

where

$$\mathbf{X} = \begin{pmatrix} \chi_\rho[\overline{(\rho)} - \overline{(\rho)^\star}] \\ \chi_{\rho u}[\overline{(\rho u_1)} - \overline{(\rho u_1)^\star}] \\ \chi_{\rho u}[\overline{(\rho u_2)} - \overline{(\rho u_2)^\star}] \\ \chi_{\rho u}[\overline{(\rho u_3)} - \overline{(\rho u_3)^\star}] \\ \chi_E[\overline{(E)} - \overline{(E)^\star}] \end{pmatrix} = \begin{pmatrix} \chi_\rho(I - Q_N \star G) \star \bar{\rho} \\ \chi_{\rho u}(I - Q_N \star G) \star \overline{\rho u_1} \\ \chi_{\rho u}(I - Q_N \star G) \star \overline{\rho u_2} \\ \chi_{\rho u}(I - Q_N \star G) \star \overline{\rho u_3} \\ \chi_E(I - Q_N \star G) \star \bar{E} \end{pmatrix}, \tag{38}$$

where χ_ρ, $\chi_{\rho u}$, and χ_E are dynamic relaxation parameters, and the operation $(I - Q_N * G)$ is used to isolate the smallest scales in the flow that can be represented by the grid. Details of the dynamic procedure for determining the parameters χ_ρ, $\chi_{\rho u}$, and χ_E can be found in Stolz et al.[6,7]

ADM using central differences and regularization by relaxation in pace of shock-capturing has been successful for moderately supersonic Mach numbers. However, the removal of small scales has the effect of creating Gibbs-like overshoots and oscillations near discontinuities; in Section IV.A we see that the relaxation regularization fares rather poorly in the case of a shocktube. As the Mach number increases, flow discontinuities grow stronger, and the problems affecting ADM with relaxation can be expected to become more severe. Here, with the eventual goal of reaching high Mach numbers, we use a dynamic Smagorinsky model along with a dynamic turbulent Prandtl number to account for the effect of the SGS scales in the ADM. The idea of using a dynamic Smagorinsky model to regularize a deconvolution model was introduced for incompressible flows by Gullbrand and Chow[18] and Winckelmans and Jeanmart.[19]

II.B.2. Regularization by Functional Modeling

The relaxation approach to regularization of the ADM equations did not use any phenomenological knowledge of the transfer of energy from represented scales to subgrid scales. Here we propose a model based on the assumption that such a transfer is carried out by a turbulent gradient diffusion process. A dynamic Smagorinksy model is derived similarly to the eddy diffusivity part of the traditional dynamic mixed model, except that here the ADM treatment for $\mathbf{T}_j^{SFS}$ takes the place of Bardina's scale-similarity model.

The SGS terms in the ADM governing equations can be written:

$$\mathbf{T}_j^{SGS} = \begin{pmatrix} \mathcal{R}_j \\ \mathcal{T}_{1j} + \delta_{1j}\mathcal{P} \\ \mathcal{T}_{2j} + \delta_{2j}\mathcal{P} \\ \mathcal{T}_{3j} + \delta_{3j}\mathcal{P} \\ \gamma c_v \mathcal{Q}_j + \frac{1}{2}\mathcal{J}_j \end{pmatrix}, \tag{39}$$

where the unclosed terms for the ADM equations are:

$$\mathcal{R}_j = \overline{(\rho u_j)} - \overline{(\rho u_j)^\star} \tag{40}$$

$$\mathcal{T}_{ij} = \overline{\rho u_i u_j} - \overline{(\rho u_i)^\star (\rho u_j)^\star / \rho^\star} \tag{41}$$

$$\mathcal{P} = (\gamma - 1)\left[\overline{E} - \overline{E^\star}\right] - \frac{1}{2}\mathcal{T}_{kk} \tag{42}$$

$$\mathcal{Q}_j = \overline{\rho u_j T} - \overline{(\rho u_j)^\star \check{T}^\star} \tag{43}$$

$$\mathcal{J}_j = \overline{\rho u_k u_k u_j} - \overline{(\rho u_k)^\star (\rho u_k)^\star (\rho u_j)^\star / (\rho^\star)^2}. \tag{44}$$

Note that no nonlinearities (with respect to the conserved variables) appear in $\mathcal{R}_j$ or in the first bracketed term of $\mathcal{P}$. We make the simplifying assumption that these are zero. The difference between a variable ϕ and its approximately defiltered counterpart $\phi^\star$ is confined to lengthscales below the Nyquist cutoff for the grid and those just above it where the deconvolution procedure cannot reconstruct the information in a reasonable number of iterations. These lengthscales in question are either completely missing from $\overline{\phi}$ (in the case of subgrid scales) or highly attenuated due to the fact that $\hat{G}(k) \to 0$ as $k \to k_{\text{Nyquist}}$. Thus, there is very little difference between $\overline{\phi}$ and $\overline{\phi^\star}$, especially for filters where $d\hat{G}(k)/dk \to 0$ as $k \to k_{\text{Nyquist}}$. This is true of the filters considered in this paper.

As in the DMM case, here we model only the SGS stresses $\mathcal{T}_{ij}$ and the SGS heat flux $\mathcal{Q}_j$. It seems plausible that, in analogy to traditional LES, these are the most important terms, but *a priori* studies of DNS data should be carried out to verify this assumption.

To derive a dynamic model, we again apply a test filter to the solution. We use a superscript circle $(\cdot)^\circ$ to denote a variable that has been defiltered with respect to the composite filter $\widehat{\overline{\cdot}}$. The SGS stresses with respect to the composite filter are

$$\mathbb{T}_{ij} = \widehat{\overline{\rho u_i u_j}} - \widehat{\overline{(\rho u_i)^\circ (\rho u_j)^\circ / \rho^\circ}}. \tag{45}$$

The ADM version of Germano's identity is then

$$\mathcal{L}_{ij}^{\mathrm{ADM}} = \mathbb{T}_{ij} - \widehat{\mathcal{T}}_{ij}, \tag{46}$$

where

$$\mathcal{L}_{ij}^{\mathrm{ADM}} = \widehat{\overline{(\rho u_i)^\star (\rho u_j)^\star / \rho^\star}} - \widehat{\overline{(\rho u_i)^\circ (\rho u_j)^\circ / \rho^\circ}}. \tag{47}$$

Applying the eddy viscosity model at the two filter levels yields

$$\mathcal{L}_{ij}^{\mathrm{ADM}} = C\beta_{ij} - \widehat{C\alpha_{ij}}, \tag{48}$$

where α_{ij} and β_{ij} are as defined for the DMM in Section II.A.2. Solving for C yields

$$C = \frac{\left\langle \mathcal{L}_{ij}^{\mathrm{ADM}} M_{ij} \right\rangle}{\left\langle M_{lk} M_{lk} \right\rangle}, \tag{49}$$

where M_{ij} is as defined above. A similar procedure for the SGS heat flux yields:

$$\frac{Pr_{\mathrm{turb}}}{C} = \frac{\left\langle M_k^T M_k^T \right\rangle}{\left\langle \mathcal{L}_j^{\mathrm{ADM},\ T} M_j^T \right\rangle} \tag{50}$$

where

$$\mathcal{L}_{ij}^{\mathrm{ADM},\ T} = \widehat{\overline{(\rho u_j)^\star T^\star}} - \widehat{\overline{(\rho u_j)^\circ T^\circ}}, \tag{51}$$

and M_{ij}^T is as defined above. Finally, the SGS terms are approximated as

$$\mathcal{T}_{ij} \approx C\alpha_{ij}, \tag{52}$$

$$\mathcal{Q}_j \approx -\frac{C}{Pr_{\mathrm{turb}}} \alpha_{ij}^T. \tag{53}$$

Note that, similarly to the case of $\tilde{T}$ in Section II, computing the quantities $T^\star$ and T° in general involves the modeled values for the SGS stresses $\mathcal{T}_{kk}$ and $\mathbb{T}_{kk}$. The one-parameter DMM provided information about the trace of τ_{ij} due to the SSM term, even though the eddy viscosity part is traceless. However, in the case of the ADM unclosed terms, the SFS part is modeled not by an SSM term but rather by modifying the convective fluxes on the left-hand side of the equations. Therefore, no analog of the SSM term appears in the model for $\mathcal{T}_{ij}$, and the modeled SGS stresses are traceless.

III. Filtering

III.A. Traditional Discrete Filtering

Recall that we define the LES filter according to a convolution:

$$\bar{u} = \int G(\vec{x}, \vec{y}) u(\vec{y}) d\vec{y} \equiv G * u. \tag{54}$$

If the filter kernel G is chosen to have compact support, then we may write a discrete representation explicitly as

$$\overline{f}_i = \sum_{k=-N}^{N} a^k f_{i+k}; \tag{55}$$

e.g.,

$$\overline{f}_i = a^{-1} f_{i-1} + a^0 f_{i+0} + a^1 f_{i+1} = \frac{1}{4} f_{i-1} + \frac{1}{2} f_{i+0} + \frac{1}{4} f_{i+1} \tag{56}$$

is a commonly used tophat filter.

We denote the filter (transfer) function (i.e., the Fourier transform of the filter kernel G with respect to y) as $\mathfrak{G}(k)$. The effect of applying the filter to a wave of wavenumber k is to multiply the signal by $\mathfrak{G}(k)$.

If the filter is symmetric, then the filter function is real, and the filter function gives the attenuation of the signal as a function of wavenumber. We define the cutoff wavenumber to be that k such that $\mathfrak{G}(k) = 1/2$.

Gullbrand[20] and Gullbrand and Chow[18] studied the benefits of explicitly versus implicitly filtered LES and concluded that explicit filtering is worthwhile for models such as ADM that reconstruct the defiltered solution to high order but that traditional models like DSM and DMM achieve better accuracy for a given computational cost when used in implicitly filtered LES. In order to make a "fair" comparison based on accuracy versus cost, we use implicit filtering for the DSM and DMM simulations and explicit filtering for the ADM simulations.

For explicitly filtered LES, we will use the filter (once in each direction) with coefficients given by (1/4, 1/2, 1/4) which approximates a tophat with width equal to twice the grid spacing. In computing dynamic model coefficients, we use a test filter with a lower cutoff wavenumber. Let us call the test filter kernel H and its filter function $\mathfrak{H}(k)$. Ideally, the composite filter $H \circ G$ should have a filter function similar to $\mathfrak{G}$ in shape but of half the width. That is, $\mathfrak{H}(k/2)\mathfrak{G}(k/2) = \mathfrak{G}(k)$. In practice, we cannot obtain a test filter that gives the exact desired composite filter function. Here we use three applications of the tophat filter to approximate the correct test filter. Figure 2 plots the filter functions of the tophat filter, the test filter and the actual and ideal composite filters. The test filter based on repeated application of the tophat filter gives a composite filter function that follows the ideal composite filter function closely for low wavenumbers and tolerably well for the entire range. We could also use the optimization procedure of Vasilyev et al.[21] to generate a test filter that gives approximately the correct composite filter function; however, such a filter would have a transfer function that crosses zero, and the approximate inversion of such a filter would fail. Since we need to defilter the test-filtered data in the proposed SGS model for ADM, we want a filter that can be inverted. The repeated application of a filter with a strictly positive filter function (up to the Nyquist wavenumber) is an easy way of generating a filter function that does not cross zero.

For implicitly filtered LES, the computation of certain terms in the DMM requires an explicit filtering operation that mimics the effect of the unknown implicit filter. Comparison with filtered DNS data also requires an assumption to be made about the shape of the implicit filter. Here we use the filter with coefficients (1/8, 3/4, 1/8) which approximates a tophat with width equal to the grid spacing. The test filter corresponding to implicit filtering is then the simple tophat with coefficients (1/4, 1/2, 1/4). Figure 3 plots the filter functions of the narrow tophat filter, the simple tophat test filter and the actual and ideal composite filters (assuming a filter width ratio of two).

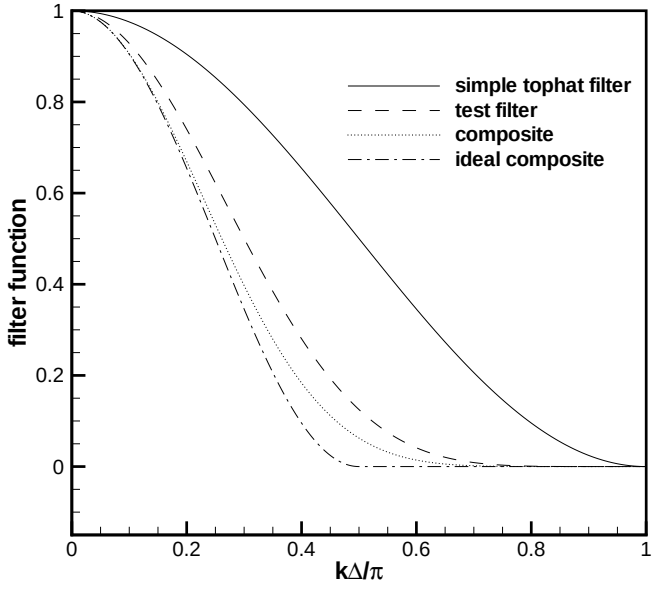

Figure 2. Filter functions for tophat LES filter with coefficients (1/4, 1/2, 1/4), test filter based on repeated application of tophat filter, and composite of the two compared to the ideal composite filter function for the tophat.

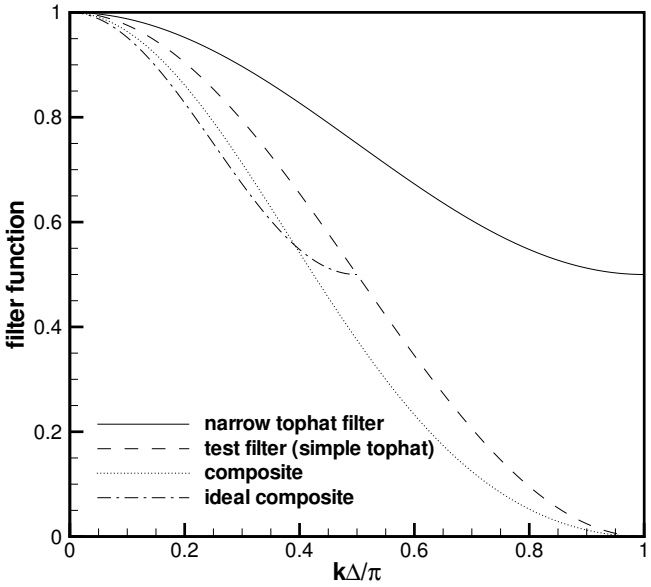

Figure 3. Filter functions for narrow tophat LES filter with coefficients (1/8, 3/4, 1/8), test filter with coefficients (1/4, 1/2, 1/4), and composite of the two compared to the ideal composite filter function.

III.B. Shock-Confining Filters

In LES of flows with shocks, we face a fundamental dilemma with regard to filtering in space. On one hand, we want to remove small turbulent scales from the solution in order to model them and thus lower the computational cost. On the other hand, discontinuities such as shocks are small scale flow features that are governed by gasdynamics, and we do not seek to model them with our turbulence models.

The discrete linear filters used in traditional LES rely on data from a stencil of fixed width centered about the grid point of interest. In the vicinity of shocks (or other discontinuities), part of the filter stencil may lie across a shock, and in general this filtering across a shock will cause smearing of the shock and/or the creation of new maxima and minima on either side of the shock. In order to avoid filtering across shocks, we use a shock-confining filter (SCF) which adapts its coefficients in response to the local smoothness of the flow solution. In order to determine where filter adaptation is warranted, the SCF uses information about the smoothness of the flow field that is already computed by the WENO shock-capturing scheme for the convective terms.

Figure 4 schematically illustrates the desired behavior of an SCF: discontinuities are unaffected, but smooth regions are filtered. By turning off the filter in discontinuous regions, we turn off the ADM scheme (or the SSM part of the DMM) and allow the underlying shock-capturing scheme to handle the parts of the flow that are predominantly governed by gasdynamics. Ideally, the SCF confines a shock to the same number of grid points that the underlying shock-capturing scheme requires to resolve a shock in the absence of any turbulence modeling.

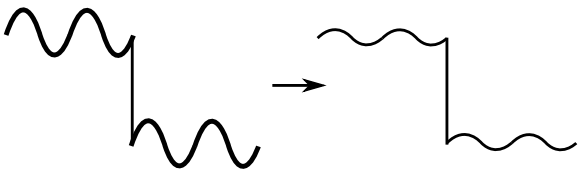

Figure 4. Ideal behavior of a shock-confining filter.

In order for the filter to adapt, its coefficients must be allowed to vary in space. We generalize the discrete

filter definition from (55) to

$$\overline{f}_i = \sum_{k=-N}^{N} b_i^k f_{i+k} = \text{e.g., } b_i^{-1} f_{i-1} + b_i^0 f_{i+0} + b_i^1 f_{i+1}. \tag{57}$$

The new subscript index refers to the grid point where the filtered value is to be calculated. The superscript continues to refer to the offset from that location. In smooth regions, the adaptation should turn off and the coefficients should reduce to their "optimal" or linear values $b_k^i = a_k$.

The WENO scheme for the convective fluxes uses a stencil built from a selection of candidate stencils around the point of interest with different biases. A measure of the degree of WENO stencil adaptation is provided by the nonlinearity index NI as given in Weirs[22] or Taylor et al.[23] Here we use the quantity that is referred to as NI' in Taylor et al.,[23] which is NI renormalized such that $NI' = 0$ indicates no adaptation, and $NI' = 1$ indicates a maximally adapted stencil. The WENO scheme adapts based on the smoothness of individual characteristic flow variables, but the SCF is applied to conserved variables. We therefore seek a single quantity that gives a measure of whether a shock exists at a particular location. If we are filtering in the x_i direction, then the NI' values corresponding to the three characteristic variables that would be involved in a shock or other discontinuity in that direction are averaged and scaled by a factor c_{NI} to give a value that we call a barrier height α. We call it a barrier height because we are notionally creating a barrier at each cell face to control the flow of information across discontinuities during filtering. The simulations actually use a finite difference code, but we will still speak in terms of cell faces in the context of SCF.

We constrain the filter adaptation to preserve two properties of the filter:

• P1–Global conservation of the variable, i.e.,

$$\sum_i \overline{f}_i = \sum_i f_i. \tag{58}$$

• P2–Preservation of constants, i.e.,

$$f_i = C, \ \forall \ i \in [a, b] \Longrightarrow \overline{f}_i = C, \ \forall \ i \in [a + N, b - N]. \tag{59}$$

In the derivation of the LES equations from the Navier-Stokes equations, we have assumed that filtering commutes with differentiation, i.e.,

$$\overline{\frac{\partial \phi}{\partial x}} = \frac{\partial \overline{\phi}}{\partial x}. \tag{60}$$

Unfortunately, this property cannot be maintained in regions of the flow where the filter is adapting. We assume that in high speed flows, the potential benefit from lessening oscillations near discontinuities outweighs the commutation error introduced by the adaptation. It follows from (57) that the filter is linear in the sense that $\overline{a\phi + b\psi} = a\overline{\phi} + b\overline{\psi}$ for scalar constants a, b and functions ϕ, ψ. We make repeated use of this fact throughout the derivation.

Consider a filter with a stencil covering the points $(i-1, i, i+1)$. For simplicity, assume a periodic domain of N_x points. Then the values b_k^i represent $3N_x$ degrees of freedom. Enforcing properties P1 and P2 imposes $2N_x$ constraints, leaving N_x degrees available for adaptation. As mentioned above, we choose to impose a barrier height $\alpha_{i+\frac{1}{2}}$ at each cell face $i + \frac{1}{2}$ such that $\alpha_{i+\frac{1}{2}} = 1$ totally prevents information from being referenced across that face and $\alpha_{i+\frac{1}{2}} = 0$ corresponds to uninhibited reference to such information. Imposing these barriers at each of the N_x cell faces makes use of the remaining degrees of freedom. Schematically, we can imagine information being partially reflected and transmitted at each cell face based on the local barrier height as in Figure 5. We can imagine an effective value of f_{i-1} that is used in calculating $\overline{f}_i$. Let $f_{i-1,i}^{\text{eff}}$ denote this effective value of f_{i-1} as "seen" from i. We choose a simple linear combination:

$$f_{i-1,i}^{\text{eff}} = (1 - \alpha_{i-1/2}) f_{i-1} + \alpha_{i-1/2} f_i. \tag{61}$$

Similarly,

$$f_{i+1,i}^{\text{eff}} = (1 - \alpha_{i+1/2}) f_{i+1} + \alpha_{i+1/2} f_i. \tag{62}$$

The effective quantities are operated on using the linear filter coefficients:

$$\overline{f}_i = \sum_{k=-N}^{N} a^k f_{i+k,i}^{\text{eff}} = \sum_{k=-N}^{N} b_i^k f_{i+k}. \tag{63}$$

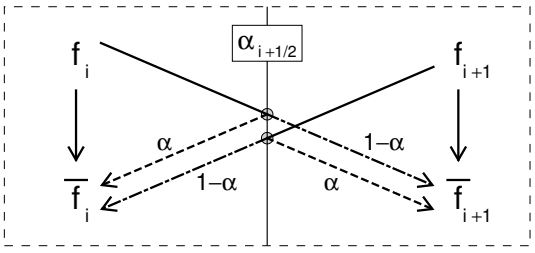

Figure 5. Notional transmission and reflection of information at a cell face barrier.

This expression can be solved for the adaptive stencil coefficients b_i^k. An adaptive filter derived in this manner automatically satisfies the desired properties P1 and P2.

In the case of linear filters, a three-dimensional filter is often implemented using the successive application of one-dimensional filters in the Cartesian basis i-, j-, and k-directions. However, in the case of the SCF, the three-dimensional filter produced in this manner would depend on the order in which the three one-dimensional filters were applied. We would like the SCF to have no preferred direction, so we effectively average the six possible permutations of the i-, j-, and k-filters. Let us denote the filter operations in the i-, j-, and k-directions as $\overline{(.)}^{\,i}_{i,j,k}$, $\overline{(.)}^{\,j}_{i,j,k}$, and $\overline{(.)}^{\,k}_{i,j,k}$, respectively. We use a, b, and c to distinguish between the filter coefficients in the three directions, and we now use three subscripts to identify the grid point at which the filtered value is to be found:

$$\overline{f}^{\,i}_{i,j,k} = \sum_{\ell=-N}^{N} \left[a^{\ell}_{i,j,k}\right] f_{i+\ell,j,k} \tag{64}$$

$$\overline{f}^{\,j}_{i,j,k} = \sum_{m=-N}^{N} \left[b^{m}_{i,j,k}\right] f_{i,j+m,k} \tag{65}$$

$$\overline{f}^{\,k}_{i,j,k} = \sum_{n=-N}^{N} \left[c^{n}_{i,j,k}\right] f_{i,j,k+n} \tag{66}$$

Applying the filters in the order i, j, k results in the expression:

$$\overline{\overline{\overline{f}}}^{\,i,j,k}_{i,j,k} = \sum_{n=-N}^{N} \sum_{m=-N}^{N} \sum_{\ell=-N}^{N} \left[c^{n}_{i,j,k} b^{m}_{i,j,k+n} a^{\ell}_{i,j+m,k+n}\right] f_{i+\ell,j+m,k+n}. \tag{67}$$

The roles of the coefficients in the bracketed portion of (67) depend on the filtering order. In order to define a three-dimensional filter without such a dependence, we define new coefficients according to

$$\begin{aligned} d_{i,j,k,\ell,m,n} \equiv \frac{1}{6} \{ & c^{n}_{i,j,k} b^{m}_{i,j,k+n} a^{\ell}_{i,j+m,k+n} + c^{n}_{i,j,k} b^{m}_{i,j+m,k+n} a^{\ell}_{i,j+m,k} \\ & + c^{n}_{i+\ell,j+m,k} b^{m}_{i,j,k} a^{\ell}_{i,j+m,k} + c^{n}_{i,j+m,k} b^{m}_{i,j,n} a^{\ell}_{i,j+m,k+n} \\ & + c^{n}_{i+\ell,j,k} b^{m}_{i+\ell,j,k+n} a^{\ell}_{i,j,k} + c^{n}_{i+\ell,j+m,k} b^{m}_{i+\ell,j,k} a^{\ell}_{i,j,k} \} \end{aligned} \tag{68}$$

Then the filtered quantity is computed as

$$\overline{\overline{\overline{f}}}^{\,3D}_{i,j,k} = \sum_{n=-N}^{N} \sum_{m=-N}^{N} \sum_{\ell=-N}^{N} \left[d_{i,j,k,\ell,m,n}\right] f_{i+\ell,j+m,k+n}. \tag{69}$$

We drop the superscript $3D$ and return to using a single overbar for the remainder of the paper.

IV. Numerical Simulations

All simulations in this paper are computed using a finite difference code to solve the governing equations in conservative form. Unless stated otherwise, the convective terms are computed using a fourth-order-accurate bandwidth-optimized symmetric WENO scheme[22,24,25] that uses four points per candidate stencil. A relative limiter is applied to the WENO smoothness index as in Taylor et al.[23] in order to improve the grid convergence properties and to prevent WENO from erroneously adapting in regions containing only turbulent fluctuations. In the case of the ADM with relaxation regularization, we use eight-point fourth-order-accurate central differences that have been bandwidth-optimized. Time integration is carried out using a low-storage third-order-accurate Runge-Kutta scheme due to Williamson.[26] Modeled fluxes appearing on the right-hand sides of governing equations are computed using fourth-order central differences, as are the viscous terms. In ADM with relaxation regularization, a smoothing filter is used in the process of computing the dynamic relaxation coefficients; we accomplish this smoothing by applying the coarse tophat with coefficients (1/4, 1/2, 1/4) three times.

IV.A. Shocktube

In order to isolate the effects of gasdynamics from those of turbulence, we first consider a shocktube problem. We choose a one-dimensional, periodic domain with 256 grid points and left and right initial states $(\rho_L, u_L, p_L) = (1\text{kg/m}^3, 0\text{m/s}, 1\text{Pa})$ and $(\rho_R, u_R, p_R) = (0.1\text{kg/m}^3, 0\text{m/s}, 0.125\text{Pa})$. At the start of the simulation, shocks, contact surfaces, and expansion waves form and propagate away from the interfaces between the left and right states. Because of the symmetry of the problem, we present results from only half of the domain. We stop the simulation before the physical waves interact, but numerical disturbances due to the ADM defiltering operation propagate faster than physical waves and do interact somewhat due to the periodic boundary condition. Other simulations with very long non-periodic domains suggest that the interaction does not qualitatively change the results.

All of the shocktube results plotted here were computed using the simple tophat filter (either linearly or in SCF form). In order to more clearly identify the extent of discontinuities as they are represented by WENO, the filter adaptation is controlled not simply by barrier heights α, but by the largest α value within the width of the WENO stencil. (i.e., $\alpha_{i+1/2}^{\text{effective}} = \max_{j=-4}^{j=+4}(\alpha_{i+j+1/2})$)

Figure 6 plots the density profile along the shocktube for an ADM simulation using central differences and relaxation regularization. Spurious oscillations develop around the discontinuities. The WENO shock-capturing method applied to a DNS (using the same grid) would almost completely remove the oscillations; however, as shown in Figure 7, WENO applied to the ADM convective terms in equation (33) does not eliminate the oscillations for an ADM simulation. Figure 8 shows that the use of the shock-confining filter with ADM largely eliminates the oscillations to within graphical accuracy.

IV.B. Decaying Isotropic Turbulence

In order to assess the shock-confining filter in turbulent flows, we first consider the problem of decaying compressible isotropic turbulence in a periodic box. We use a nominal initial Taylor microscale Reynolds number of $Re_\lambda = 50$ and nominal initial turbulent Mach number $M_t = q/a_{\text{avg}}$ of 1.5. The initial field is advanced using DNS on 192^3 grid points until $t = 6\lambda/u'_{\text{rms}}$, at which time it is linearly filtered onto 32^3 grid points. At $t = 6\lambda/u'_{\text{rms}}$, the flow parameters have decayed to $Re_\lambda = 23$, $M_t = 0.66$, and $M'_{\text{rms}} = 0.27$, and the coarse grid resolves 73% and 57% of turbulent kinetic energy for the implicit LES (DSM and DMM) and explicit LES (ADM) cases, respectively. All runs except for the ADM with relaxation use WENO. The ADM with relaxation uses central differences following Stolz et al.[6,7]

Figure 9 plots instantaneous density contours at $t = 6\lambda/u'_{\text{rms}}$. Steep gradients indicating the presence of shocklets are clearly visible.

Figure 10 compares the decay of resolved turbulent kinetic energy (TKE) for the implicitly filtered LES cases (DSM and DMM) against filtered DNS data. Although the figure compares a single realization of LES against a single realization of DNS, which should not be expected to agree except in a statistical sense, the domain contains approximately $4^3 = 64$ large scale eddies, so we expect the comparison to be meaningful. Jiménez[27] explains that in dynamic models, the energy of small scales adjusts until the dissipation matches the production at the test filter scale. This leads to a vertical offset in TKE decay curves after some transient adjustment period. In Figure 10 we estimate that this occurs by $t = 8\lambda/u'_{\text{rms}}$, after which the

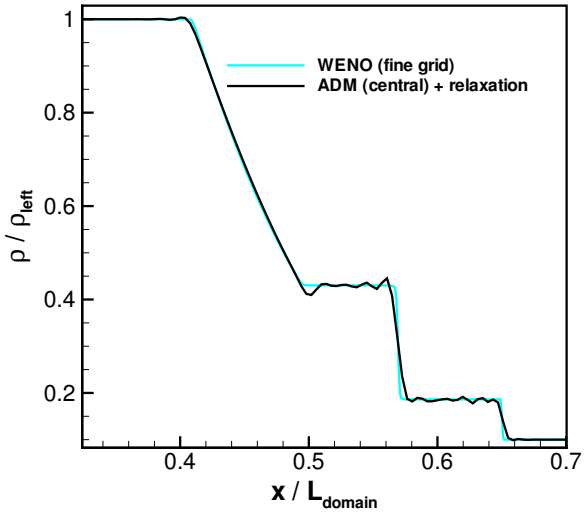

Figure 6. Instantaneous density profile in shocktube simulation using ADM with relaxation regularization on 256 grid points compared with WENO (non-ADM) calculation on 1024 grid points.

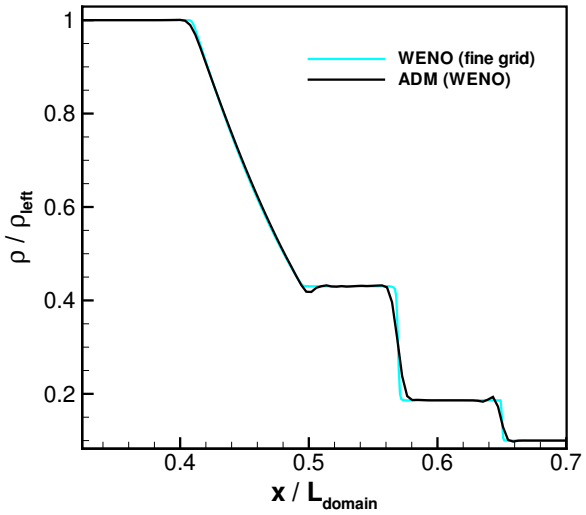

Figure 7. Instantaneous density profile in shocktube simulation using ADM with WENO and linear filter on 256 grid points compared with WENO (non-ADM) calculation on 1024 grid points.

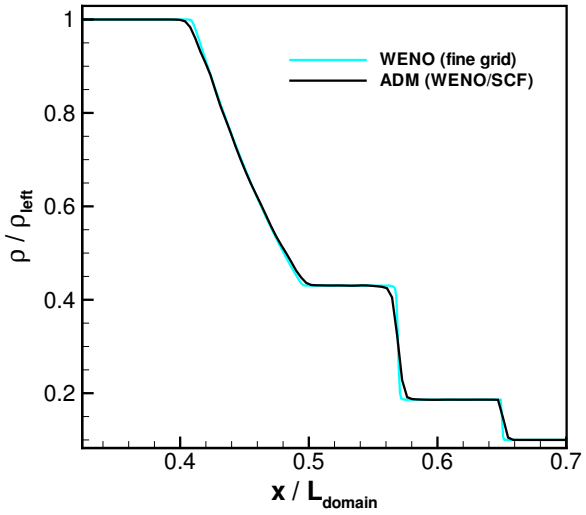

Figure 8. Instantaneous density profile in shocktube simulation using ADM with WENO and shock-confining filter on 256 grid points compared with WENO (non-ADM) calculation on 1024 grid points.

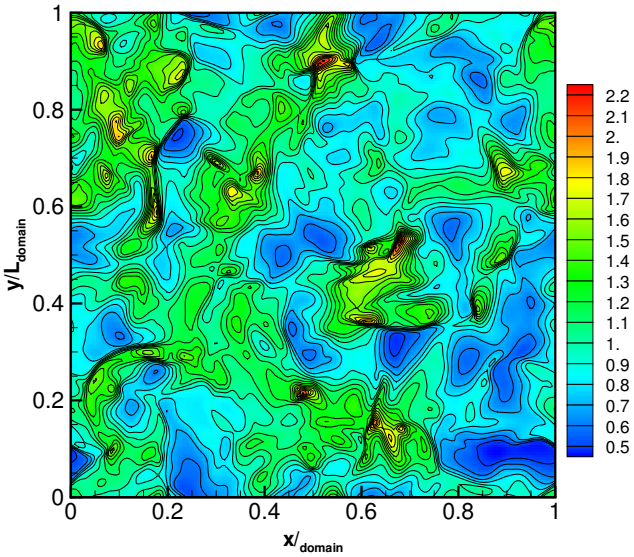

Figure 9. DNS density contours ρ/ρ_{avg} at $t = 6\lambda/u'_{\rm rms}$ at which LES runs were started from filtered DNS data. The instantaneous state is described by $Re_\lambda = 23$ and $M_t = 0.66$.

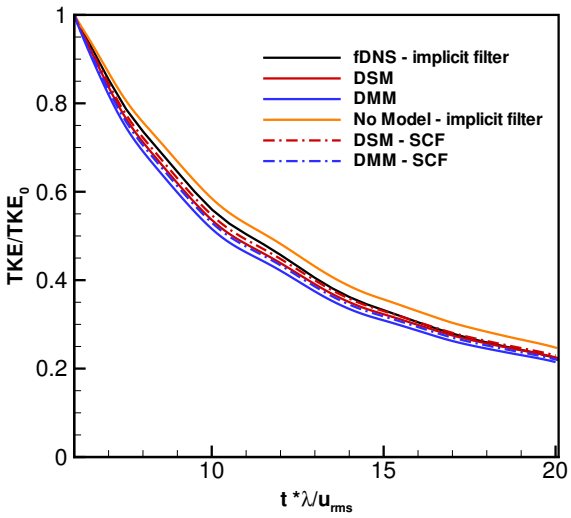

Figure 10. Decay of resolved turbulent kinetic energy in LES of isotropic turbulence using dynamic Smagorinsky and mixed models. Large-eddy simulations were started from a realistic DNS solution with $Re_\lambda = 23$ and $M_t = 0.66$. At the start of the LES, 73% TKE is resolved. Filtered DNS data is plotted for comparison, as is a no-model run.

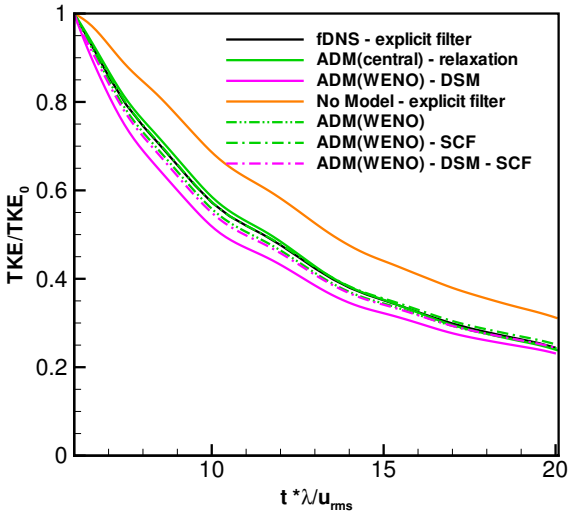

Figure 11. Decay of resolved turbulent kinetic energy in LES of isotropic turbulence using approximate deconvolution models with and without dynamic regularization via relaxation terms and DSM. Dot-dashed lines indicate the use of shock-confining filter. Dot-dot-dashed line indicates ADM using WENO without regularization. Large-eddy simulations were started from a realistic DNS solution with $Re_\lambda = 23$ and $M_t = 0.66$. At the start of the LES, 57% TKE is resolved. Filtered DNS data is plotted for comparison, as is a no-model run.

curves move roughly in parallel. The downward offset of the DSM and DMM models indicate that they are more dissipative than the ideal. The no-model curve exhibits an upward offset corresponding to less dissipation than ideal. Replacing the linear filter with a shock-confining filter (using $c_{NI} = 0.5$ and without using the maximum α over the WENO stencil) decreases the overly dissipative nature of the models but does not appear to interfere with their ability to dynamically adjust to the correct dissipation rate.

Figure 11 compares the decay of resolved turbulent kinetic energy (TKE) for the explicitly filtered LES cases (ADM) against filtered DNS data. Here the ADM with DSM regularization is overly dissipative, while the ADM with relaxation regularization is slightly under dissipative. Because the simulation starts with DNS data that has been filtered using the coarser explicit grid filter, the upward offset of the no-model curve is much greater than before. As before, replacing the linear filter with SCF reduces the dissipation. Also plotted are curves representing ADM using WENO without additional regularization. Here the switch to SCF makes the decay curve closely match the filtered DNS. Note that because the simulation used an arbitrarily chosen value of $c_{NI} = 0.5$, the excellent agreement may be partly fortuitous, but it at least demonstrates that WENO with ADM is not inherently overly dissipative when SCF is used. Furthermore, the combination of WENO and ADM without further regularization already provides adequate dissipation, and this may cast doubt on the benefit of the DSM regularization presented above. More effort toward correctly linking the degree of filter adaptation to the WENO adaptation in general cases might potentially result in a model with both non-oscillatory shock-capturing capability and proper dissipation levels.

To assess the importance of the turbulence models relative to the numerical dissipation, we quantify the dissipation rate contributions due to the SGS model (or regularization part of ADM), to viscosity, and to the convective terms (in ADM or traditional form and using WENO or central differences). This is accomplished by turning off the appropriate terms and then running a single, very small time step and noting the changes in dissipation of resolved TKE over that time step. The dissipation budgets are computed at $t = 8\lambda/u'_{\text{rms}}$ when time the transient adjustment period is finished.

In Table 1, we see that in the DSM and DMM simulations the dissipation due to the WENO shock-capturing scheme is not negligible, but it is significantly less than that due to the SGS models. Because of the compressibility of the flow and the possibility of shocklets still existing at $t = 8\lambda/u'_{\text{rms}}$, it is possible that the level of numerical dissipation is appropriate. The dissipation of the convective terms in ADM is due to the combined action of the numerical method and the deconvolution procedure, and these cannot be separated. However, we can still see that the dissipation due to the dynamic relaxation regularization is significantly larger than that due to ADM with central differences. The ADM with DSM regularization used WENO and therefore can be expected to have higher dissipation due to the convective terms. However, the fact that the dynamic Smagorinsky regularization term adjusts its coefficient to provide significant dissipation is a sign that the convective (and viscous) terms by themselves are not overly dissipative. The main lesson from the dissipation budgets is that, while we do not know how much dissipation is due to physically correct shocklet events, we at least can see that the dissipation due to the turbulence models is not overwhelmed by that of the shock-capturing scheme.

Model	SGS (%)	Viscous (%)	WENO (%)
DSM(WENO)	26.9	53.2	19.8
DMM(WENO)	36.2	49.6	14.2

	relaxation (%)	Viscous (%)	Central + ADM (%)
ADM(CD)-relaxation	42.8	31.3	26.0

	SGS (%)	Viscous (%)	WENO + ADM (%)
ADM(WENO)-DSM	23.7	40.1	36.2

Table 1. LES Dissipation Breakdown

The computational cost in terms of CPU seconds per timestep relative to a coarse DNS using WENO

(or "no-model" LES) is tabulated for each model in Table 2 . For the current problem size (32^3), the coarse DNS takes 0.660 seconds on 8 Beowolf nodes with dual 2.20GHz Intel XEON(TM) CPUs. The simulation from $t = 6\lambda/u'_{\rm rms}$ to $t = 20\lambda/u'_{\rm rms}$ requires 96 steps, and this is similar for all models. For comparison, to continue the 192^3 DNS over the same time period would be roughly 900 times more expensive than the ADM with relaxation. The ADM with relaxation is the least expensive model primarily because it avoids the use of a shock-capturing scheme and it involves fewer filtering operations than the other models (except for the unregularized ADM with WENO). The remaining models in order of increasing number of filtering operations are DSM, DMM, and then ADM with DSM regularization. The switch from linear to shock-confining filters is also expensive, and the cost of this clearly increases as the fraction of the total computational cost that is due to filtering operations increases. In the simple isotropic case considered here, there is no apparent benefit to using the more expensive DMM over DSM, nor to using the DSM to regularize the ADM. Although shock-confining filters also increase the cost, they do at least provide a more correct dissipation level in these cases.

Model	Regularization	Filter	CPU time
No-Model (WENO)			1.00
ADM (central)	relaxation	linear	1.52
ADM (WENO)		linear	1.88
ADM (WENO)		SCF	2.40
ADM (WENO)	DSM	linear	7.04
ADM (WENO)	DSM	SCF	11.70
DSM (WENO)		linear	2.60
DSM (WENO)		SCF	3.15
DMM (WENO)		linear	3.91
DMM (WENO)		SCF	4.96

Table 2. Computational cost of various models relative to a coarse DNS (or no-model LES).

IV.C. Forced Isotropic Turbulence

The forcing scheme of Overholt and Pope[28] for isotropic turbulence is used to maintain a steady state and allow tests in a more strongly compressible turbulent flow. Because we are using the forcing scheme in a compressible flow, we introduce a thermal energy removal term to prevent the build up of thermal energy over time as energy is continually fed to the largest scales and ultimately dissipated as heat. The forcing acts in wavenumber space and amplifies the lowest wavenumber modes without changing their phases. The forcing scheme adds energy as needed to prevent the computed energy spectrum from falling significantly below a model or target spectrum, $E_m(\kappa)$. Each mode evolves in time according to the differential equation

$$\frac{\partial \hat{\mathbf{u}}(\boldsymbol{\kappa}, t)}{\partial t} = \hat{\mathbf{a}}(\boldsymbol{\kappa}, t) + \frac{f_\kappa(t)}{\tau_f}\hat{\mathbf{u}}(\boldsymbol{\kappa}, t)$$

where $\hat{\mathbf{a}}(\boldsymbol{\kappa}, t)$ is the Fourier transform of the usual Navier-Stokes equation terms, $f_\kappa(t)$ is the forcing coefficient for the Fourier modes in the κ-shell, and τ_f is the forcing timescale. The coefficients $f_\kappa(t)$ evolve according to

$$\frac{\mathrm{d}f_\kappa(t)}{\mathrm{d}t} = P\left[\frac{-1}{\tau_f}\ln\left(\frac{E(\kappa,t)}{E_m(\kappa)Z_f(\kappa)}\right) - \alpha\alpha_c f_k(t)\right] = P\left[S_\kappa\right]$$

where α is a dimensionless damping parameter (taken here to be 1), $\alpha_c = 2\sqrt{2}/\tau_f$ is the damping coefficient giving critical damping, and P is an operator defined by

$$P\left[S_\kappa\right] = \begin{cases} S_\kappa \text{ for } f_\kappa \geq 0 \\ S_\kappa \text{ for } f_\kappa = 0 \text{ and } S_\kappa > 0 \\ 0 \text{ for } f_\kappa = 0 \text{ and } S_\kappa \leq 0 \end{cases}$$

The forcing cut-off function $Z_f(\kappa)$ is defined by

$$Z_f(\kappa;\kappa_f,\zeta) = \tanh\left(\frac{\kappa_f - \kappa}{\zeta\kappa_f}\right) H(\kappa_f - \kappa)$$

where κ_f is the wavenumber at which the forcing goes to zero, and, in this paper, $\zeta = 0.2$. The forcing timescale is related to the Kolmogorov timescale by the dimensionless parameter

$$T_f^* = \left(\frac{\tau_f}{\tau_\eta}\right)$$

which is here taken to be $T_f^* = 0.3$.

In order to prevent a steady increase in average temperature due to the addition of energy via forcing, we compute the total energy added by the forcing term at each timestep subtract this amount from the conservation equation for total energy in a spatially uniform manner. This holds the total energy of the flow constant while still preserving the local changes in energy due to forcing. The results appear to be insensitive to the details of the energy removal. Simulations run with the local rate of thermal energy removal matched to the local rate of energy addition gave nearly identical results.

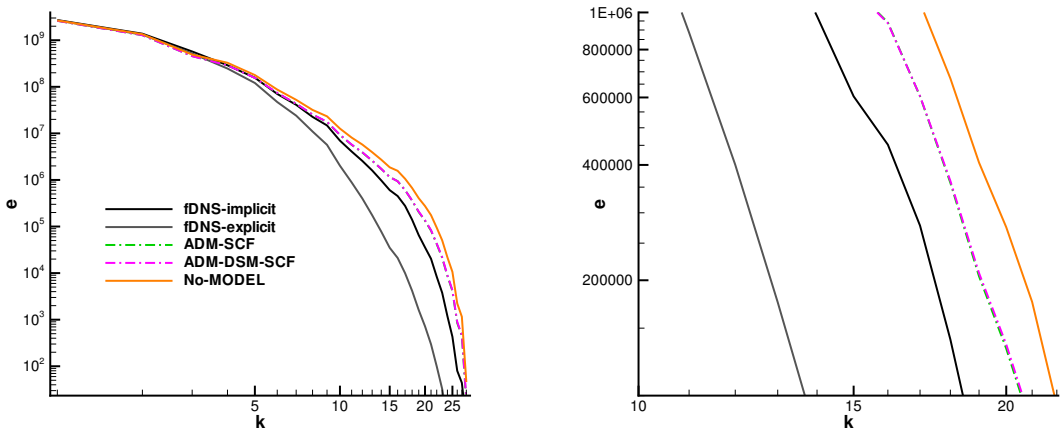

(a) (b) Zoomed in view. Line legend as in 12(a)

Figure 12. Spectra in forced isotropic turbulence computed using ADM with and without regularization via DSM. Dot-dashed lines indicate the use of shock-confining filter. Large-eddy simulations were started from a forced DNS solution with $Re_\lambda = 52$, $M_t = 1.05$i, and $M'_{\rm rms} = 0.46$. At the start of the LES, 87% TKE is resolved on the coarse filter and 92% is resolved by the fine filter. Filtered DNS data is plotted for comparison, as is a no-model run. The curve for ADM without regularization is partially obscured by the curve for ADM with DSM regularization.

The LES of forced isotropic turbulence is performed on a 32^3 grid and is started from a forced DNS on a 64^3 grid with $Re_\lambda = 52$, $M_t = 1.05$, and $M'_{\rm rms} = 0.46$. The forced DNS is forced (until $t = 100\lambda/u'_{\rm rms}$) toward a model spectrum that is equal to the instantaneous spectrum of the decaying isotropic turbulence at the instant the forcing was turned on. The LES is forced toward the (filtered) spectrum of the forced DNS taken at the instant that the DNS solution is filtered onto the LES grid. The forced turbulence (or rather the decaying turbulence from which it was started) was initialized with an energetic eddy length scale equal to the domain side length, so the domain contains only approximately a single energetic eddy. Therefore, in order to obtain statistical results, we average the spectra from $t = 120\lambda/u'_{\rm rms}$ to $t = 300\lambda/u'_{\rm rms}$.

At the start of the LES, 87% TKE is resolved by the coarse tophat filter and 92% is resolved by the fine tophat filter. These results are preliminary in that the criterion for choosing the filter cutoff wavenumber was to have as much separation as possible between the forced wavenumbers and the subfilter scale wavenumbers so that the effects of forcing and modeling would not directly interact. We use $\kappa_f = 4$ so that the forcing acts only up to the $|\kappa_f| = 3$ shell. The cutoff wavenumber for the explicit filter is $\kappa = 8$, and that for the

implicit filter is $\kappa = 16$. This separation is questionably small and would be made worse if we attempted an LES with a higher fraction of unresolved TKE. Future investigations will use higher Reynolds numbers to optimize the separation between forced and filtered scales while increasing the amount of TKE in the unresolved scales.

In this section we focus on ADM because of the cost effectiveness that would results from its possible lack of need for regularization beyind that provided by using WENO for shock-capturing. Figure 12 plots spectra for forced LES. The implicitly and explicitly filtered DNS spectra are plotted for comparison. It is unclear whether a reasonable comparison can be made between LES and DNS because the spectra are computed from $\tilde{u}$ which by definition depends on the filter used. In the case of the SCF, the filter adapts and in turn changes the interpretation of the solution $\tilde{u}$. The DNS data have been filtered using linear filters. If the SCF were not to adapt at all, then we could compare the LES spectra with linearly filtered DNS spectra. As the SCF adapts, it does less filtering (at all scales, but especially at the smallest scales), and therefore the LES spectra should (and do) lie above that of the filtered DNS. Making any more precise statement about a target result is difficult. Comparisons between LES models can be made, but it should be remembered that the LES resolves almost all of the TKE and therefore is approaching a DNS.

The ADM with linear filters (not shown) is unstable both using central differences with relaxation regularization and using WENO with DSM regularization. The shock-confining filter successfully stabilizes the ADM, both with and without DSM regularization. The spectra from the ADM simulations are similar to those of DSM and DMM using linear filters (not shown). Despite using the explicit filtering approach, ADM appears to accumulate amounts of energy in the higher wavenumbers similar to that in LES using the traditional implicitly filtered approach. The ADM, even without regularization, is more dissipative than the no-model simulation. This is probably because of two facts. First the turbulence cascade transfers energy toward lower wavenumbers where the explicit filter attenuates it. There is no such explicit filtering in the no-model simulation. Second, the deconvolved solution $u^\star$ is less smooth than $\tilde{u}$ and contains more high wavenumber content which causes WENO to adapt more. The DSM regularization term has little effect in this test case. It may be that the domain contains so many shocklets that the SCF adapts almost everywhere and that this effectively turns off the DSM term.

V. Conclusions

We have proposed a new shock-confining filtering method for LES of compressible flows that separates turbulent scales into resolved and unresolved parts but avoids filtering shocks and other discontinuities. Numerical simulations of the shocktube problem show that use of this new filter eliminates the spurious oscillations that appear in ADM simulations with relaxation regularization. It therefore shows promise for shock/turbulence interaction simulations.

Numerical simulations of decaying isotropic turbulence show that the use of the shock-confining filter reduces the excessive dissipation of the DSM and DMM as well as ADM with DSM regularization. Although the relatively inexpensive ADM with relaxation gives very accurate results in decaying turbulence, in problems with strong shocks such as shock/turbulent-boundary-layer interaction problems, it may be advantageous to accept the greater expense of the ADM with SCF or the greater expense and slightly inferior performance of the DMM with SCF in order to avoid smearing of the strong shock and spurious oscillations in its vicinity.

Simulations of forced isotropic turbulence show that the use of the shock-confining filter stabilizes the ADM, both with and without DSM regularization. ADM with regularization only via the WENO dissipation produces a spectrum nearly identical to that of ADM regularized by DSM. This suggests that the more expensive DSM regularization may not be worthwhile and that ADM using WENO may be a viable model without additional regularization. However, here the SCF may be adapting to such an extent that the explicit filter simply has little effect, and this would of course partially turn off the DSM regularization. The DSM regularization might still be needed in smoother regions in turbulent flows where WENO adapts less and therefore provides less dissipation, such as away from the strong shock in an STBLI problem. Although the ADM without additional regularization was successful in the decaying isotropic turbulence case, that case used $c_{NI} = 0.5$ and did not use the maximum barrier height over the WENO stencil. That version of the SCF was not robust enough in the forced case, and so the success of the ADM/WENO/SCF combination in both cases cannot be interpretted as proof that the method is generally applicable in the same form across all ranges of compressibility. More investigation is needed on this point. If this method can be made generally

applicable, in addition to offering better treatment of shocks, it could offer attractive computational cost. The ADM with SCF is 2.40 times as expensive as a no-model simulation compared to 2.60 times for DSM or 3.91 times for DMM with linear filtering. If the trends found in incompressible flow also hold here, the ADM should also offer greater accuracy on a given grid, making it preferable to DSM and DMM.

Acknowledgments

This work is sponsored in part by AFOSR Grant FA9550-06-1-0323 and NASA CUIP Award NCC3-989. Computational resources were provided by the CRoCCo Laboratory at Princeton University.

References

[1]Germano, M., Piomelli, U., Moin, P., and Cabot, W. H., "A dynamic subgrid-scale eddy viscosity model," *Phys. Fluids A*, Vol. 3(7), 1991, pp. 1760–1765.

[2]Lilly, D. K., "A proposed modification of the Germano subgrid-scale closure method," *Phys. Fluids A*, Vol. 4(3), March 1992, pp. 633–635.

[3]Bardina, J., Ferziger, J. H., and Reynolds, W. C., "Improved Subgrid Scale Models for Large Eddy Simulation," AIAA paper 80–1357, Aug. 1980.

[4]Vreman, B., Geurts, B., and Kuerten, H., "On the formulation of the dynamic mixed subgrid-scale model," *Phys. Fluids*, Vol. 6(12), December 1994, pp. 4057–4059.

[5]Stolz, S. and Adams, N., "An approximate deconvolution procedure for large-eddy simulation," *Phys. Fluids*, Vol. 11(7), December 1999, pp. 1699–1701.

[6]Stolz, S., Adams, N. A., and Kleiser, L., "An approximate deconvolution model for large-eddy simulation with application to incompressible wall-bounded flows," *Phys. Fluids*, Vol. 13(4), 2001, pp. 997–1015.

[7]Stolz, S., Adams, N. A., and Kleiser, L., "The approximate deconvolution model for large-eddy simulations of compressible flows and its application to shock-turbulent-boundary-layer interaction," *Phys. Fluids*, Vol. 13(10), 2001, pp. 2985–3001.

[8]Harten, A., Engquist, B., Osher, S., and Chakravarthy, S. R., "Uniformly High Order Accurate Essentially Non-Oscillatory Schemes III," *Journal of Computational Physics*, Vol. 71, No. 2, 1987, pp. 231–303.

[9]Shu, C.-W. and Osher, S., "Efficient Implementation of Essentially Non-Oscillatory Shock-Capturing Schemes II," *Journal of Computational Physics*, Vol. 83, No. 1, 1989, pp. 32–78.

[10]Liu, X.-D., Osher, S., and Chan, T., "Weighted Essentially Non-Oscillatory Schemes," *Journal of Computational Physics*, Vol. 115, No. 1, 1994, pp. 200–12.

[11]Jiang, J.-S. and Shu, C.-W., "Efficient Implementation of Weighted ENO Schemes," *Journal of Computational Physics*, Vol. 126(1), 1996, pp. 202–228.

[12]Martín, M. P., Piomelli, U., and Candler, G. V., "Subgrid-Scale Models for Compressible Large-Eddy Simulations," *Phys. Fluids*, Vol. 13(11), November 2001, pp. 3400–3410.

[13]Smagorinsky, J., "General circulation experiments with the primitive equations: I. The basic experiment." *Mon. Weather Rev.*, Vol. 91, 1963, pp. 99–164.

[14]Moin, P., Squires, K., Cabot, W., and Lee, S., "A dynamic subgrid-scale model for compressible turbulence and scalar transport," *Phys. Fluids A*, Vol. 3(11), 1991, pp. 2746–2757.

[15]Comte, P. and Lesieur, M., "Large-eddy simulation of compressible turbulent flows." *Advances in Turbulence Modeling*, edited by D. Olivari, Von Karman Institute for Fluid Dynamics, 1998, pp. 4:1–4:133.

[16]Speziale, C. G., Erlebacher, G., Zang, T. A., and Hussaini, M. Y., "The subgrid-scale modeling of compressible turbulence," *Phys. Fluids*, Vol. 31(4), 1988, pp. 940–942.

[17]van Cittert, P. H., "Zum Einfluß der Spaltbreite auf die Intensitatsverteilung in Spektrallinien II," *Zeitschrift für Physik*, Vol. 69, 1931, pp. 298–308.

[18]Gullbrand, J. and Chow, F. K., "The effect of numerical errors and turbulence models in large-eddy simulations of channel flow, with and without explicit filtering," *J. Fluid Mech.*, Vol. 495, 2003, pp. 323–341.

[19]Winckelmans, G. S. and Jeanmart, H., "Assessment of some models for LES without/with explicit filtering," *Direct and Large-Eddy Simulation IV*, edited by B. J. Geurts, R. Friedrich, and O. Métais, Kluwer, 2001, pp. 55–66.

[20]Gullbrand, J., "Explicit filtering and subgrid-scale models in turbulent channel flow," *CTR Annual research briefs*, 2001, pp. 31–43.

[21]Vasilyev, O. V., Lund, T. S., and Moin, P., "A General Class of Commutative Filters for LES in Complex Geometries," *J. Comp. Phys.*, Vol. 46, 1998, pp. 82–104.

[22]Weirs, V. G., "A Numerical Method for the Direct Simulation of Compressible Turbulence," *Ph.D. thesis, University of Minnesota*, December 1998.

[23]Taylor, E. M., Wu, M., and Martín, M. P., "Optimization of Nonlinear Error for Weighted Essentially Non-Oscillatory Methods in Direct Numerical Simulations of Compressible Turbulence," *Journal of Computational Physics*, in press as of November 2006.

[24]Weirs, V. G. and Candler, G. V., "Optimization of weighted ENO schemes for DNS of compressible turbulence," AIAA paper 1997–1940, 1997.

[25]Martín, M. P., Taylor, E. M., Wu, M., and Weirs, V. G., "A Bandwidth-Optimized WENO Scheme for the Direct Numerical Simulation of Compressible Turbulence," *Journal of Computational Physics*, Vol. 220(1), 2006, pp. 270–289.

[26]Williamson, J. H., "Low-storage Runge-Kutta Schemes," *Journal of Computational Physics*, Vol. 35, No. 1, 1980, pp. 48–56.

[27]Jiménez, J., "On why dynamic subgrid-scale models work," *CTR Annual Research Briefs*, 1995, pp. 25–34.

[28]Overholt, M. R. and Pope, S. B., "A Deterministic Forcing Scheme for Direct Numerical Simulations of Turbulence," *Computers and Fluids*, Vol. 27, No. 1, 1998, pp. 11–28.